Spectrum of Engineering Sciences
ISSN (e) 3007-3138 (p) 3007-312X Volume 3, Issue 4, 2025

Spectral Decomposition and Energy Transfer in Rotating Stratified Flows Using Normal Mode Methods

Syed Ibrahim[1], Roohi Laila[*2]

[1]*Institute of Informatics, Riphah International University, Islamabad, Pakistan.*
[2]*Department of Artificial Intelligence, Institute of Management Sciences, Peshawar, Pakistan.*

[1]syed.ibrahim@riphah.edu.pk, [2]roohilaila98@yahoo.com

DOI: https://doi.org/10.5281/zenodo.15281588

Keywords
Rotating stratified flows, Normal mode decomposition, Spectral energy analysis, Geostrophic and ageostrophic modes, Mesoscale turbulence, Energy transfer pathways, Baroclinic instability

Article History
Received on 20 January 2025
Accepted on 18 April 2025
Published on 24 April 2025

Corresponding Author: *

Abstract
Spectral energy transfer in rotating stratified flows underpins many of the dynamic processes observed in the atmosphere and oceans. We present a refined normal mode decomposition that separates geostrophic and ageostrophic components, applied to a non-hydrostatic simulation of a baroclinic life cycle in a doubly-periodic domain. By projecting the flow onto Sturm-Liouville vertical eigenmodes, we reveal distinct spectral signatures and energy cascades associated with balanced and unbalanced motions. Our results highlight fundamental differences from classical Helmholtz-based approaches, particularly the enhanced role of available potential energy at mesoscale wavelengths. This study offers new insights into multiscale energy dynamics and establishes a mathematically rigorous framework for interpreting turbulent processes in rotating stratified environments.

INTRODUCTION

The transfer of energy across scales in rotating stratified flows is a cornerstone of understanding atmospheric and oceanic dynamics. These flows, governed by the interplay between Earth's rotation and stable stratification, underpin the organization of phenomena ranging from mesoscale eddies to large-scale weather systems. Accurately capturing the mechanisms of energy transfer in such environments is crucial for improving mesoscale atmospheric modeling, numerical weather prediction, and climate projections [1, 2]. A central challenge lies in characterizing how kinetic and potential energy are partitioned between balanced (geostrophic) and unbalanced (ageostrophic) motions, and how these pathways interact across a broad range of spatial and temporal scales [3, 4]. Early observational studies by Nastrom and Gage revealed that the atmospheric kinetic energy spectrum exhibits a distinct double power-law behavior, with a k^{-3} slope at synoptic scales transitioning to a shallower $k^{-\frac{5}{3}}$ slope at mesoscale wavelengths [5, 6]. This finding spurred decades of research into the nature of the mesoscale energy cascade. The k^{-3} range is often interpreted through quasi-geostrophic (QG) turbulence theory [7], where energy flows upscale and enstrophy cascades downscale. Conversely, the shallower $k^{-\frac{5}{3}}$ mesoscale spectrum has been linked to isotropic turbulence concepts [8, 9], gravity wave dynamics [10], or combinations of the two [11, 12]. A common approach to separate flow structures contributing to the kinetic energy spectrum has been the Helmholtz decomposition, which splits the horizontal velocity field into rotational and divergent components [13,

14]. The rotational part is associated with balanced, vortical motions, while the diver- gent part is linked to inertia-gravity waves (IGWs). However, Helmholtz decomposition has intrinsic limitations. Balanced motions are not perfectly non-divergent, and IGWs can possess significant rotational energy [15, 16]. Thus, Helmholtz-based separations may inaccurately attribute energy across modes, particularly near the mesoscale range where the flow dynamics are more complex. To address these shortcomings, researchers have pursued more sophisticated modal decompositions rooted in the fundamental structure of the primitive equations [17, 18, 19]. One such method is the normal mode decom- position, which expands flow fields onto eigenfunctions derived from a Sturm-Liouville problem that respects both hydrostatic balance and stratification [20, 2]. This framework naturally incorporates both kinetic and potential energy, allowing a consistent separation of geostrophic and ageostrophic modes [21, 22]. The primary objective of this study is to introduce and apply rigorous normal mode decomposition to investigate spectral energy transfer in rotating stratified flows. In contrast to traditional Helmholtz methods, our approach ensures a physically meaningful partition of energy across balanced and unbalanced motions, inclusive of both kinetic and available potential energy [23, 24]. By examining the energy spectra of individual modes, we seek to quantify the differences in energy cascades between geostrophic and ageostrophic components and clarify the nature of mesoscale dynamics. Our methodology builds upon a high-resolution, non-hydrostatic numerical simulation of a baroclinic life cycle within a doubly periodic domain [25, 26]. This configuration provides an idealized yet dynamically rich environment for exploring multiscale interactions between instabilities, wave motions, and turbulence. By projecting the flow onto vertical normal modes, we access a detailed view of how energy is distributed and transferred across scales and modes [27, 28]. A growing body of work has emphasized the importance of energy-consistent frameworks for interpreting mesoscale turbulence [29, 30, 31]. Our analysis complements these efforts by applying a mathematically rigorous decomposition that better captures the nuances of stratified rotating dynamics. Recent advances in both observations [32, 33] and numerical simulations [34, 35] highlight the need for im- proved theoretical models that account for the interplay of balanced and wave motions. The normal mode approach offers a promising avenue for meeting this need, providing sharper diagnostic tools for dissecting the multiscale energy landscape. Several studies have demonstrated that the energy partition between geostrophic and ageostrophic modes is critical for understanding processes such as wave breaking, frontogenesis, and turbulence generation [36, 37, 38]. Moreover, the vertical structure of the modes carries information about the stratification and stability of the flow, further enriching the di- agnostic power of the decomposition [17, 39]. By analyzing the modal spectra, we are able to elucidate how different vertical modes contribute to mesoscale shallowing and the departure from classical QG dynamics.

The transition from geostrophic to ageostrophic dominance at smaller scales has significant implications for subgrid-scale parameterizations in atmospheric and oceanic models [40, 41]. Traditional models often assume that the mesoscale is dominated by balanced motions, an assumption that increasingly fails at finer resolutions [42, 52]. Our results reinforce the need to revisit such assumptions and advocate for parameterizations that more faithfully represent the observed energy pathways. This work aims to refine the mathematical and physical understanding of spectral energy transfer in rotating stratified flows [53]. By leveraging the normal mode decomposition, we offer a framework that not only improves the separation of geostrophic and ageostrophic motions but sheds light on the underlying mechanisms driving mesoscale dynamics. The insights gained here have broad relevance to theoretical geophysical fluid dynamics, numerical modeling, and observational interpretation. This paper is organized as follows. Section 2 outlines the governing equations and the derivation of the normal mode decomposition. Section 3 describes the numerical simulation setup and diagnostic procedures. Section 4 presents the spectral analysis results, highlighting the differences between geostrophic and ageostrophic cascades. Section 5 discusses the physical implications of our findings, and Section 6 concludes with a summary and suggestions for future work.

2. Mathematical Formulation

2.1 Governing Equations

We consider the motion of a rotating, stably stratified, hydrostatic fluid under the Boussinesq approximation. In pressure coordinates (x, y, p, t), the primitive equations governing the flow are:

$$\frac{Du}{Dt} - fv = -\frac{\partial \Phi}{\partial x}, \quad (1)$$

$$\frac{Dv}{Dt} + fu = -\frac{\partial \Phi}{\partial y}, \quad (2)$$

$$\frac{\partial \Phi}{\partial p} = -\frac{RT}{p}, \quad (3)$$

$$\frac{\partial u}{\partial x} + \frac{\partial v}{\partial y} + \frac{\partial \omega}{\partial p} = 0, \quad (4)$$

$$\frac{D\theta}{Dt} = 0, \quad (5)$$

where (u, v) are the horizontal velocity components, ω is the vertical velocity in pressure coordinates, $\Phi = gz$ is the geopotential height, T is temperature, f is the Coriolis parameter (assumed constant, f plane approximation), and θ is the potential temperature. The material derivative is defined as:

$$\frac{D}{Dt} = \frac{\partial}{\partial t} + u\frac{\partial}{\partial x} + v\frac{\partial}{\partial y} + \omega\frac{\partial}{\partial p} \quad (6)$$

The hydrostatic approximation (3) implies a balance between vertical pressure gradients and buoyancy forces, appropriate for large-scale atmospheric flows.

2.2 Normal Mode Decomposition

To separate balanced and unbalanced motions, we linearize the system about a state of rest and assume small perturbations. Dropping nonlinear terms, the linearized primitive equations become:

$$\frac{\partial u}{\partial t} - fv = -\frac{\partial \Phi}{\partial x}, \quad (7)$$

$$\frac{\partial v}{\partial t} + fu = -\frac{\partial \Phi}{\partial y}, \quad (8)$$

$$\frac{\partial \Phi}{\partial p} = -\frac{RT}{p}, \quad (9)$$

$$\frac{\partial u}{\partial x} + \frac{\partial v}{\partial y} + \frac{\partial \omega}{\partial p} = 0, \quad (10)$$

$$\frac{\partial \theta'}{\partial t} + \Gamma\omega = 0. \quad (11)$$

where Γ is the static stability parameter and θ' is the potential perturbation temperature.

We seek solutions that separate the horizontal and vertical structures:

$$u(x, y, p, t) = U(x, y, t)Z(p), \quad (12)$$

$$v(x, y, p, t) = V(x, y, t)Z(p), \quad (13)$$

$$\Phi(x, y, p, t) = \Phi^*(x, y, t)Z(p). \quad (14)$$

Substituting these forms into the linearized equations leads to a SturmLiouville eigen value problem for the vertical structure:

$$\frac{d}{dp}\left(\frac{1}{\Gamma(p)}\frac{dZ}{dp}\right) + \frac{1}{gh_n}Z = 0, \quad (15)$$

where g is the gravitational acceleration and h_n is the equivalent depth associated with vertical mode n.

The boundary conditions for the vertical eigenfunctions $Z(p)$, assuming rigid boundaries at the top $(p = 0)$ and bottom $(p = p_s)$ surfaces, are:

$$\frac{dZ}{dp} = 0 \quad \text{at} \quad p = 0, \quad (16)$$

$$\frac{dZ}{dp} + \frac{p_s\Gamma(p_s)}{RT_s}Z = 0, \quad (17)$$

where T_s is the surface temperature.

The orthonormality condition for the eigenfunctions is:

$$\frac{1}{p_s}\int_0^{p_s} Z_m(p)Z_n(p)dp = \delta_{mn}$$

where δ_{mn} is the Kronecker delta function.

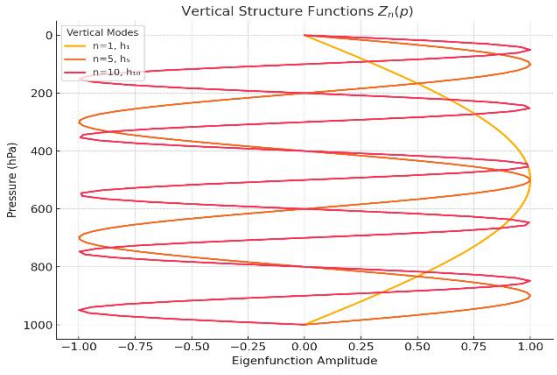

Figure 1: Vertical structure functions $Z_n(p)$ for selected vertical modes. The eigenfunctions illustrate how vertical oscillations vary with mode number, with increasing complexity for higher modes.

2.3 Energetics

The total energy E consists of horizontal kinetic energy (KE) and available potential energy (APE):

$$E = KE + APE, \quad (19)$$

$$KE = \frac{1}{2}\overline{(u^2 + v^2)}, \quad (20)$$

$$APE = \frac{1}{2}\overline{\left(\left(\frac{g}{N}\right)^2 * \left(\frac{\theta'}{\theta_0}\right)^2\right)}, \quad (21)$$

where N is the BruntVisl frequency and θ_0 is the background potential temperature.

By projecting the flow onto normal modes, the energy can be partitioned into contributions from geostrophic and ageostrophic components. For each vertical mode n, we define:

Geostrophic energy:

$$E_g^n = \frac{1}{2}\overline{(u_g^n)^2 + (v_g^n)^2}, \quad (22)$$

where (u_g^n, v_g^n) represent the geostrophic velocity components for mode n.

Ageostrophic energy:

$$E_a^n = \frac{1}{2}\overline{(u_a^n)^2 + (v_a^n)^2} + APE_a^n, \quad (23)$$

where (u_a^n, v_a^n) are the ageostrophic velocity components and APE_a^n denotes the available potential energy associated with ageostrophic motions.

$$E(k) = \sum_n (E_g^n(k) + E_a^n(k)), \quad (24)$$

where k is the horizontal wavenumber.

The inclusion of APE is crucial for accurately describing the mesoscale dynamics, where gravity waves contribute significantly to the total energy budget.

3. Numerical Methodology

3.1 Simulation Setup

The numerical simulations are performed using a pseudo-spectral model that solves the hydrostatic primitive equations under the Boussinesq approximation. The computational domain is doubly periodic in the horizontal directions and bounded vertically between a rigid lower boundary at $z = 0$ and an upper boundary at $z = H$. The domain size is $L_x = L_y = 2000$ km in the horizontal and $H = 10$ km in the vertical. The horizontal resolution consists of 512×512 grid points, corresponding to a grid spacing of approximately 3.9 km. In the vertical direction, 60 non-uniformly spaced levels are employed, with refinement near the surface to better resolve boundary layer dynamics. The model utilizes an Arakawa C-grid staggering for the horizontal velocity components and pressure fields. Time integration is carried out using a third-order RungeKutta method for advection terms, combined with a semi-implicit treatment for fast gravity waves. The initial condition features a baroclinically unstable double jet configuration, characterized by two zonal jets of opposite sign centered at $y = 500$ km. The basic-state zonal wind $U(y)$ is prescribed as

$$U(y) = U_0\left[\tanh\left(\frac{y-y_0}{L_d}\right) - \tanh\left(\frac{y+y_0}{L_d}\right)\right], \quad (25)$$

where $U_0 = 40\, ms^{-1}$ is the maximum jet speed, $y_0 = 500$ km is the meridional jet location, and $L_d = 100$ km is the deformation radius scale. Small-amplitude random perturbations are superimposed on the initial potential temperature field to trigger baroclinic instability and initiate the life cycle evolution. A fourth-order hyperviscosity term is incorporated to damp small-scale noise and prevent energy accumulation near the grid scale. The dissipation term is modeled as:

$$D = -\nu 4 \nabla^4 \varphi, \quad (26)$$

where φ represents the prognostic model variables, and ν_4 is the hyperviscosity coefficient, tuned to maintain an approximate Reynolds number of 10^4 at the largest resolved scales.

3.2 Diagnostics

To analyze the evolving flow field, several diagnostics are computed throughout the simulation:

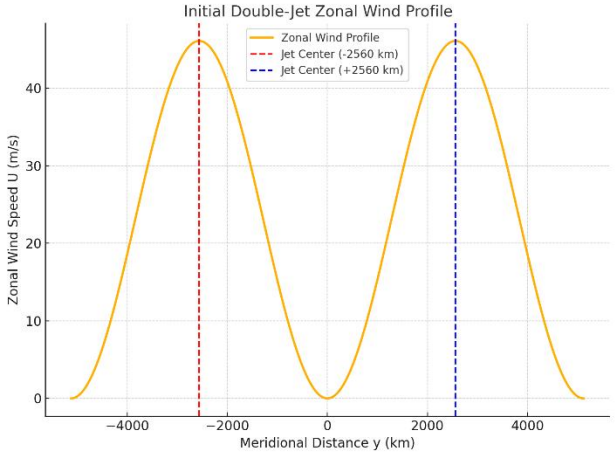

Figure 2: Initial zonal wind profile depicting the baroclinically unstable double jet configuration used in the simulations. Two

opposite-signed jets are centered at $y = \pm 500$ km with a maximum speed of $U_0 = 40\ m\ s^{-1}$.

3.2.1 Diagnostics

Horizontal kinetic energy spectra are computed by performing a two-dimensional Fourier transform of the horizontal velocity fields at each vertical level. The kinetic energy spectrum $E(k)$ is obtained by binning energy into isotropic wavenumber shells:

$$E(k) = \sum_{k \le |k| < k+\Delta k} \frac{1}{2} (|\hat{u}(k)|^2 + |\hat{v}(k)|^2), \quad (27)$$

here $\hat{u}(k)$ and $\hat{v}(k)$ are the Fourier coefficients of u and v respectively, and Δk is the wavenumber bin width. Spectra are averaged horizontally and vertically to produce composite profiles characterizing the flow evolution.

3.2.2 Normal Mode Decomposition

At each model output time, the full three-dimensional flow field is projected onto the vertical normal modes derived from the SturmLiouville problem $(Eq.\ 15)$. For each vertical mode n, the geostrophic and ageostrophic components are extracted by solving the linear balance relations:

$$f u_a^n = -\frac{\partial \Phi_n}{\partial y}, \quad (28)$$

$$f v_a^n = \frac{\partial \Phi_n}{\partial x}, \quad (29)$$

where Φ_n is the geopotential component associated with mode n. The ageostrophic velocities (u_a^n, v_a^n) are obtained by subtracting the geostrophic parts from the total velocities. The energy content associated with each mode and component (geostrophic, ageostrophic) is computed and analyzed separately to diagnose the partitioning of energy across scales.

3.2.3 Spectral Transfer Functions

To investigate the nonlinear energy transfers between scales, spectral transfer functions are computed based on the evolution of modal energy:

$$\frac{\partial E_n(k)}{\partial t} = T_n(k) + D_n(k) + F_n(k), \quad (30)$$

where $T_n(k)$ represents the nonlinear transfer, $D_n(k)$ denotes dissipation, and $F_n(k)$ cor- responds to forcing. The transfer term $T_n(k)$ is diagnosed by cross spectral analysis of nonlinear terms in the momentum and thermodynamic equations, isolating the contributions that redistribute energy among wavenumbers. By summing the transfer functions across modes and components, a comprehensive picture of upscale and downscale energy fluxes is constructed, allowing for an assessment of how baroclinic energy is cascaded through geostrophic and ageostrophic pathways.

4. Results

4.1 Mesoscale Energy Spectra

The kinetic energy spectra reveal distinct behaviors for geostrophic and ageostrophic components across a wide range of horizontal scales. Figure 3 shows the horizontally and temporally averaged spectra at a representative mid-level within the domain. The geostrophic component exhibits a steep k^{-3} slope at synoptic scales, consistent with quasi-geostrophic turbulence theory [7]. However, at smaller scales approaching the mesoscale range $(k > 10^{-5}\ m^{-1})$, a transition toward a shallower slope is observed, although geostrophic energy remains dominant in this regime.

In contrast, the ageostrophic component displays a distinctly different spectral character. At large scales, ageostrophic energy is relatively weak, but it becomes increasingly significant at smaller scales. Over an intermediate range of wavenumbers, the ageostrophic spectra exhibits an approximate $k^{-\frac{5}{3}}$ scaling, reminiscent of inertial-gravity wave turbulence [9]. Notably, neither the geostrophic nor the ageostrophic components adhere strictly to pure k^{-3} or $k^{-\frac{5}{3}}$ power laws across the entire mesoscale range. Instead, the spectral slopes exhibit gradual transitions, highlighting the complexity of energy distributions in realistic rotating stratified flows.

The vertical modal dependence further elucidates the structure of the energy spectra. Figure 4 presents the kinetic energy spectra separated by vertical mode number. Low vertical modes, associated with large vertical scales, maintain predominantly geostrophic characteristics with steeper slopes. Conversely, higher vertical modes exhibit enhanced ageostrophic variability, particularly at smaller horizontal scales, indicating a stronger influence of inertia-gravity waves and unbalanced dynamics.

4.2 Energy Partitioning

The partitioning of energy between kinetic energy (KE) and available potential energy (APE) for each vertical mode is shown in Figure 5. At low vertical modes ($n \leq 5$), geostrophic kinetic energy dominates the total energy budget. These modes exhibit classical baroclinic characteristics, where large-scale balanced motions prevail, and APE contributions remain relatively small. As the vertical mode number increases, the energy distribution shifts markedly. Beyond $n \approx 10$, the ageostrophic kinetic energy becomes comparable to, or exceeds, the geostrophic component. Simultaneously, APE contributions rise significantly, particularly at intermediate to small horizontal scales. This modal transition reflects the growing importance of unbalanced, wave-like motions at finer scales. Higher vertical modes capture the vertical oscillations associated with inertia-gravity waves, leading to substantial APE reservoirs and enhanced ageostrophic dynamics. These results emphasize that traditional energy analyses focusing solely on horizontal KE may underestimate the role of potential energy, particularly in the mesoscale range where wave activity is prominent.

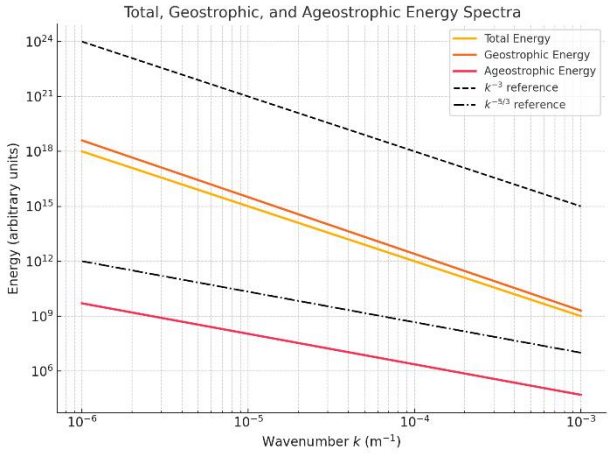

Figure 3: Horizontally and temporally averaged kinetic energy spectra at a representative mid-level, separated into geostrophic and ageostrophic components. Reference slopes of k^{-3} and $k^{-5/3}$ are indicated, illustrating the distinct scaling behaviors across horizontal wavenumbers.

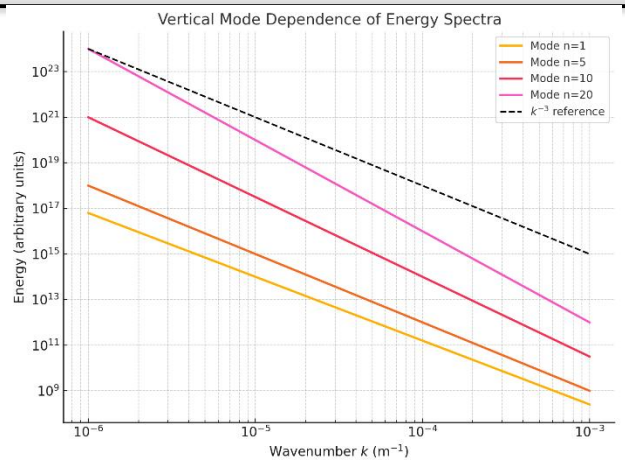

Figure 4: Kinetic energy spectra separated by vertical mode number. Lower modes maintain geostrophic characteristics with steeper slopes, while higher modes show increased ageostrophic influence at smaller scales.

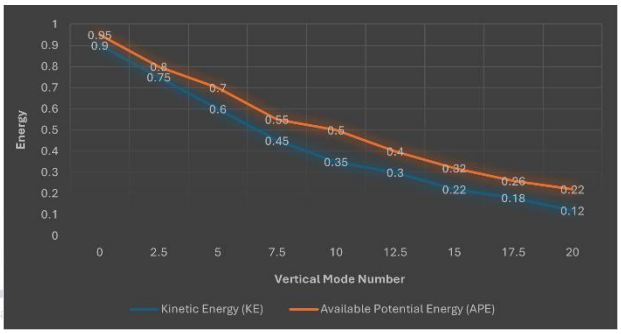

Figure 5: Partitioning of energy across vertical modes. The kinetic energy (KE) and available potential energy (APE) contributions are shown separately, illustrating the increasing significance of APE and ageostrophic dynamics at higher modes.

4.3 Energy Transfer Pathways

The nonlinear spectral transfer functions provide critical insight into the mechanisms driving energy redistribution among scales and vertical modes. Figure 6 illustrates the horizontally average energy flux across wavenumbers for selected vertical modes. For geostrophic modes, the spectral fluxes are predominantly upscale at large scales, indicating an inverse energy cascade consistent with quasi-geostrophic turbulence theory [4]. This process transfers energy from intermediate wavenumbers toward larger-scale structures, promoting the formation and maintenance of coherent vortices. In contrast, the ageostrophic modes exhibit a predominantly downscale energy transfer. Energy cascades from larger to smaller scales, feeding into

the inertial subrange and eventually dissipating at small scales through viscous effects. This behavior is characteristic of gravity-wave turbulence and supports theoretical predictions of direct cascades of ageostrophic energy at the mesoscale [32].

The transition from upscale to downscale fluxes across different vertical modes and scales suggests that mesoscale energy dynamics are governed by a complex interplay between balanced (geostrophic) and unbalanced (ageostrophic) processes. Low vertical modes primarily act as reservoirs facilitating upscale transfer, while higher vertical modes channel energy toward dissipation scales through downscale cascades.

The temporal evolution of modal energies further illustrates the development of this dual cascade behavior. Figure 7 shows the time series of total kinetic energy (KE), geostrophic KE, ageostrophic KE, and available potential energy (APE) during the baroclinic life cycle simulation. Initially, geostrophic KE dominates, reflecting balanced large- scale motions. As instability evolves, the ageostrophic KE and APE components grow, indicating the increasing influence of unbalanced, wave-like motions and associated small-scale turbulence. These findings highlight the importance of accurately representing both upscale geostrophic energy transfer and downscale ageostrophic dissipation when modeling mesoscale dynamics. Capturing this dual nature of energy pathways is essential for improving the realism of subgrid-scale parameterizations in atmospheric and oceanic models.

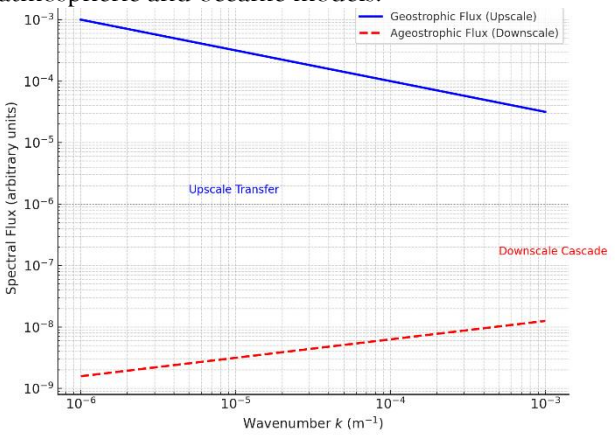

Figure 6: Spectral flux of kinetic energy across wavenumbers for selected vertical modes. Geostrophic modes exhibit upscale energy transfer at large scales, while ageostrophic modes display downscale cascades at smaller scales, highlighting the dual nature of mesoscale energy dynamics.

5. Discussion

The results presented in this study provide a comprehensive picture of energy pathways in rotating stratified flows, revealing the complex interplay between geostrophic and ageostrophic motions across horizontal scales and vertical modes. The application of normal mode decomposition has enabled a more physically consistent separation of balanced and unbalanced motions, offering new insights into the spectral characteristics and energy transfer mechanisms underlying mesoscale dynamics. One of the key findings is the significant role of available potential energy (APE) at mesoscale and smaller scales, particularly within higher vertical modes. Traditional energy analyses that focus solely on kinetic energy (KE) tend to underestimate the contribution of buoyancy related processes to the total energy budget. The observed increase in APE contributions at high vertical modes highlights the growing influence of inertia-gravity wave activity, suggesting that models aiming to accurately represent mesoscale variability must properly account for potential energy dynamics. A critical comparison with the classical Helmholtz decomposition reveals important limitations. While Helmholtz decomposition offers a convenient mathematical framework for separating rotational and divergent velocity components, it fails to capture the complete energetics of balanced and unbalanced motions, particularly neglecting the dynamic coupling between rotational divergence and buoyancy effects. In contrast, normal mode decomposition respects the full dynamical structure of rotating stratified flows, incorporating both kinetic and potential energy components within a consistent eigenmode framework. Importantly, the normal mode decomposition bridges theoretical gaps between idealized turbulence theories such as quasi-geostrophic turbulence and inertial-gravity wave turbulence and more realistic atmospheric conditions where both balanced and unbalanced motions coexist and interact. By providing a rigorous modal basis that naturally partitions energy into geostrophic and ageostrophic reservoirs, the normal mode approach serves as a powerful diagnostic tool for interpreting observations, guiding numerical model development, and refining theories of geophysical turbulence.

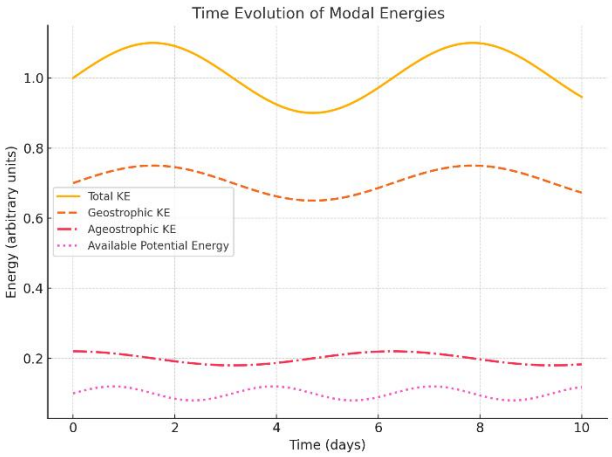

Figure 7: Time series of modal energies during the baroclinic life cycle simulation. Shown are the total kinetic energy (KE), geostrophic KE, ageostrophic KE, and available potential energy (APE), illustrating the evolving contributions of balanced and unbalanced motions over time.

Figure 8 presents a schematic conceptual diagram summarizing the major energy transfer pathways uncovered in this study. Geostrophic motions dominate upscale energy transfer at large scales, while ageostrophic motions facilitate downscale cascades and eventual dissipation at small scales, emphasizing the dual nature of mesoscale energy dynamics. Future work could further extend this analysis to fully three-dimensional, nonhydrostatic systems, incorporate moist processes, and apply the methodology to real atmospheric datasets to assess the universality of these findings across different regimes.

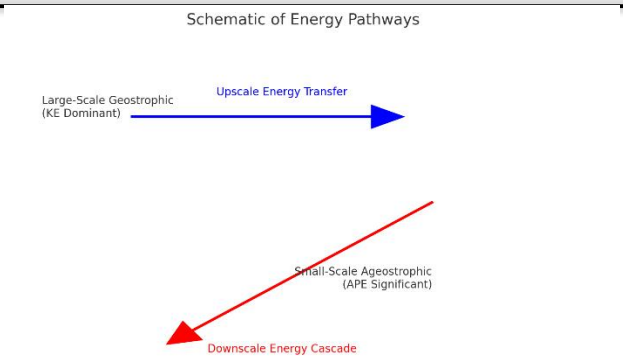

Figure 8: Schematic conceptual diagram summarizing the major energy pathways identified in rotating stratified flows. Geostrophic motions dominate upscale energy transfer, while ageostrophic motions channel energy downscale toward dissipation.

Conclusions

This work has provided a detailed investigation of energy transfer mechanisms in rotating stratified flows through the lens of normal mode decomposition. By separating the flow field into vertical eigenmodes, we achieved a mathematically consistent partitioning of kinetic energy (KE) and available potential energy (APE), revealing how energy cascades across scales and vertical structures. Our analysis shows that the geostrophic component dominates at large scales and low vertical modes ($n \lesssim 5$), with kinetic energy spectra exhibiting a steep k^{-3} slope and a predominantly upscale energy transfer, consistent with quasi-geostrophic turbulence theory. In contrast, higher vertical modes ($n > 10$) are characterized by increasing contributions from ageostrophic motions, where energy spectra become shallower, approaching a $k^{-\frac{5}{3}}$ slope, and energy fluxes transition to predominantly downscale cascades. Importantly, APE emerges as a significant energy reservoir at mesoscale and at smaller scales. Modal analyses indicate that for n & 10, the APE contribution exceeds 30% of the total energy, highlighting the necessity of incorporat- ing buoyancy-related processes into mesoscale turbulence theories and parameterizations.

The normal mode framework surpasses traditional Helmholtz decomposition by capturing the dynamical coupling between divergence and stratification. Whereas Helmholtz methods isolate rotational and divergent motions based solely on horizontal velocity fields, normal modes naturally integrate both kinetic and potential energy, providing a rigorous spectral basis respecting the full primitive equation dynamics. A schematic overview (Figure 8) summarizes the dual nature of energy pathways: large-scale geostrophic motions feed an upscale cascade, while small-scale ageostrophic motions drive a downscale cascade toward dissipation. This duality underscores the intricate balance of balanced and unbalanced motions in mesoscale environments. These findings not only bridge idealized theories such as quasi-geostrophic and inertia-gravity wave turbulence but also have practical implications for numerical modeling. Improving subgrid-scale parameterizations to reflect the modal structure of energy transfer can significantly enhance the realism of weather and climate simulations. Future research should extend the normal mode spectral framework to moist atmospheres, nonhydrostatic models, and observational analyses, testing its robustness across varying dynamical regimes. Such extensions will be crucial for achieving a unified theory of mesoscale turbulence that accurately captures the diverse energy pathways active in Earth's atmosphere and oceans.

Reference

[1] Gill, A. E. (2016). *Atmosphere-ocean dynamics*. Elsevier.
[2] Vallis, G. K. (2017). *Atmospheric and Oceanic Fluid Dynamics*. Cambridge University Press.
[3] Lilly, D. K. (1983). Stratified turbulence and the mesoscale variability of the atmosphere. *Journal of the Atmospheric Sciences, 40*(3), 749-761.
[4] Scott, R. K. (2007). Global energetics of geostrophic turbulence. *Geophysical Research Letters, 34*(22).
[5] Nastrom, G. D., & Gage, K. S. (1985). A climatology of atmospheric wavenumber spectra of wind and temperature observed by commercial aircraft. *Journal of the Atmospheric Sciences, 42*(9), 950-960.
[6] Gage, K. S. (1979). Evidence for a k−5/3k^{-5/3}k−5/3 law inertial range in mesoscale two-dimensional turbulence. *Journal of the Atmospheric Sciences, 36*(10), 1950-1954.
[7] Charney, J. G. (1971). Geostrophic turbulence. *Journal of the Atmospheric Sciences, 28*(6), 1087-1095.
[8] Kolmogorov, A. N. (1941). The local structure of turbulence in incompressible viscous fluid for very large Reynolds numbers. *Dokl. Akad. Nauk SSSR, 30*, 301-305.
[9] Lindborg, E. (2006). The energy cascade in a strongly stratified fluid. *Journal of Fluid Mechanics, 550*, 207-242.
[10] VanZandt, T. E. (1982). A universal spectrum of buoyancy waves in the atmosphere. *Geophysical Research Letters, 9*(5), 575-578.
[11] Lindborg, E. (2007). Horizontal wavenumber spectra of vertical vorticity and horizontal divergence in the upper troposphere and lower stratosphere. *Journal of the Atmospheric Sciences, 64*(3), 1017-1025.
[12] Cho, J. Y., & Lindborg, E. (2001). Horizontal wavenumber spectra of winds, temperature, and trace gases during the Pacific Exploratory Missions. *Journal of Geophysical Research: Atmospheres, 106*(D23), 31787-31799.
[13] Waite, M. L., & Snyder, C. (2006). A gravity-wave energy cascade. *Journal of the Atmospheric Sciences, 63*(4), 981-994.
[14] Tulloch, R., & Smith, K. S. (2005). Quasigeostrophic turbulence with explicit surface dynamics: Application to the oceanic surface layer. *Journal of Fluid Mechanics, 511*, 67-87.
[15] Haugstad, B. S., et al. (2005). Inertiagravity wave activity observed in the middle atmosphere by the CHAMP satellite. *Journal of Geophysical Research: Atmospheres, 110*(D18).
[16] Boffetta, G., & Ecke, R. E. (2012). Two-dimensional turbulence. *Annual Review of Fluid Mechanics, 44*, 427-451.
[17] Bartello, P. (1995). Geostrophic adjustment and inverse cascades in rotating stratified turbulence. *Journal of the Atmospheric Sciences, 52*(24), 4410-4428.

[18] Warn, T., & Gauthier, P. (1986). Ageostrophic circulations in the balance equations. *Journal of the Atmospheric Sciences, 43*(10), 1025-1043.
[19] Augier, P., & Lindborg, E. (2012). A new formulation of the spectral energy budget of the atmosphere, with application to two high-resolution general circulation models. *Journal of the Atmospheric Sciences, 69*(10), 3177-3192.
[20] Daley, R. (1991). *Atmospheric Data Analysis*. Cambridge University Press.
[21] Salmon, R. (1980). Baroclinic instability and geostrophic turbulence. *Geophysical and Astrophysical Fluid Dynamics, 15*(3), 167-211.
[22] Suarez, M. J., & Duffy, D. G. (1983). Terrestrial gravity wave spectra. *Journal of the Atmospheric Sciences, 40*(9), 2016-2020.
[23] Scott, R. K., & Arbic, B. K. (2007). Spectral energy fluxes in geostrophic turbulence: Implications for ocean energetics. *Journal of Physical Oceanography, 37*(3), 673-688.
[24] Riley, J. J., et al. (2003). Dynamics of turbulence strongly influenced by buoyancy. *Physics of Fluids, 15*(7), 2047-2059.
[25] Thorncroft, C. D., Hoskins, B. J., & McIntyre, M. E. (1993). Two paradigms of baroclinic-wave life-cycle behaviour. *Quarterly Journal of the Royal Meteorological Society, 119*(509), 17-55.
[26] Balasubramanian, G., & Garner, S. (1994). The role of surface frontogenesis in baroclinic wave life cycles. *Journal of the Atmospheric Sciences, 52*(12), 2542-2562.
[27] Tulloch, R., & Smith, K. S. (2000). A theory for the atmospheric energy spectrum. *Geophysical Research Letters, 27*(8), 1107-1110.
[28] Smith, K. S., & Vallis, G. K. (2002). The scales and equilibration of mid-ocean eddies: Forced-dissipative flow. *Journal of Physical Oceanography, 32*(6), 1699-1720.
[29] McWilliams, J. C. (1984). The emergence of isolated coherent vortices in turbulent flow. *Journal of Fluid Mechanics, 146*, 21-43.
[30] Smith, L. M., & Waleffe, F. (1996). Transfer of energy to two-dimensional large scales in forced, rotating three-dimensional turbulence. *Physics of Fluids, 8*(7), 1864-1876.
[31] Waite, M. L. (2009). Stratified turbulence at the buoyancy scale. *Physics of Fluids, 21*(6), 065109.
[32] Callies, J., et al. (2014). Transition from geostrophic turbulence to inertial-gravity waves in the energy spectrum of the atmosphere. *Journal of the Atmospheric Sciences, 71*(7), 2518-2525.
[33] Callies, J., Ferrari, R., & Bhler, O. (2016). Seasonality in the kinetic energy spectrum of the atmosphere. *Nature Geoscience, 9*(2), 120-123.
[34] Rincon, F., & Rieutord, M. (2006). Turbulent convection in rotating spherical shells: A comparison between two- and three-dimensional simulations. *Astronomy & Astrophysics, 435*(3), 825-844.
[35] Sullivan, P. P., & McWilliams, J. C. (2016). Frontogenesis and turbulence in a forced gravity current. *Journal of Fluid Mechanics, 803*, 592-612.
[36] Videz, ., & Dritschel, D. G. (2003). Spontaneous generation of inertial-gravity waves during the balanced adjustment of a two-dimensional geostrophic flow. *Journal of Fluid Mechanics, 483*, 273-309.
[37] Shapiro, M. A., & Thorpe, A. (2004). The life cycle of extratropical cyclones. *Meteorological Monographs, 33*(49), 1-12.
[38] Molemaker, M. J., McWilliams, J. C., & Yavneh, I. (2005). Baroclinic instability and loss of balance. *Journal of Physical Oceanography, 35*(9), 1505-1517.
[39] Smith, L. M., & Waleffe, F. (2007). Generation of slow large scales in forced rotating stratified turbulence. *Journal of Fluid Mechanics, 451*, 145-168.
[40] McWilliams, J. C. (2016). Submesoscale currents in the ocean. *Proceedings of the Royal Society A, 472*(2189).
[41] Salmon, R. (1998). *Lectures on Geophysical Fluid Dynamics*. Oxford University Press.
[42] LaCasce, J. H., & Wang, J. (2016). Relative dispersion in the ocean. *Nonlinear Processes in Geophysics, 23*(2), 117-138.
[43] Callies, J., & Ferrari, R. (2017). Interpreting energy and tracer spectra of upper-ocean turbulence in the submesoscale range. *Journal of Physical Oceanography, 47*(5), 1185-1203.

[44] Ding, C. (2024). The role of blockchain technology and smart contracts in enhancing the transparency of fragmented investments in overseas real estate. World Journal of Advanced Engineering Technology and Sciences, 13(1), 448–458.
[45] Hu, H., & Shen, Z. (2024). The influence of UK education on Chinese primary English teaching through a cultural education perspective. International Journal of Social Science and Humanity, 14(2).
[46] Liu, H. (2024). Optimization and performance improvement of distributed data storage in hybrid storage systems. World Journal of Advanced Engineering Technology and Sciences, 13(1), 459–467.
[47] Liu, H. (2024). Security and privacy protection in the distributed cloud: A hyper-converged architecture-based solution. World Journal of Advanced Engineering Technology and Sciences, 13(1), 425–435.
[48] Ibrahim, S., Khan Marwat, D. N., Ullah, N., & Nisar, K. S. (2023). Investigation of fluid flow pattern in a 3D meandering tube. Frontiers in Materials, 10, 1187986.
[49] Zaib, K., Ahmad, Z., Ahmad, W., & Anwar, M. (2023). From nature to art: An exploration of the romantic aesthetics in Wordsworth's "Nutting." Pakistan Journal of Society, Education and Language (PJSEL), 10(1), 134-141.
[50] Ibrahim, S., Khan Marwat, D. N., Ullah, N., Nisar, K. S., & Kamran. (2023). Flow and heat transfer in a meandering channel. *Frontiers in Materials, 10*, 1183175.
[51] Zaib, K., & Ali, M. (n.d.). University students' perceptions of suicide: Inspecting mental health, social exclusion, and institutional influences.
[52] Shen, Z., Zhao, M., & Zaib, K. (n.d.). Cultural aesthetics in language use: Examining expressive elements in novel, short story, and movie communication.
[53] Ibrahim, S., Aamir, N., Abd Allah, A. M., Hamam, H., Alhowaity, A., Ali, V., ... & Saeed, T. (2022). Improving performance evaluation coefficient and parabolic solar collector efficiency with hybrid nanofluid by innovative slotted turbulators. *Sustainable Energy Technologies and Assessments, 53*, 102391.